Experimental determination of the permeability of textiles: A benchmark exercise

René Arbter, Jean-Marc Béraud, Christophe Binetruy, Laurent Bizet, Joël Bréard, Sébastien Comas-Cardona, Cristian Demaria, Andreas Endruweit, Paolo Ermanni, Frank Gommer, et al.

Experimental determination of the permeability of textiles: A benchmark exercise

R. Arbter [a], J.M. Beraud [b], C. Binetruy [c], L. Bizet [d], J. Bréard [d], S. Comas-Cardona [c], C. Demaria [e], A. Endruweit [f,*], P. Ermanni [a], F. Gommer [g], S. Hasanovic [h], P. Henrat [b], F. Klunker [i], B. Laine [j], S. Lavanchy [k], S.V. Lomov [g], A. Long [f], V. Michaud [k], G. Morren [l], E. Ruiz [e], H. Sol [l], F. Trochu [e], B. Verleye [g], M. Wietgrefe [h], W. Wu [i], G. Ziegmann [i]

[a] *Centre of Structure Technologies, Eidgenössische Technische Hochschule Zürich, Switzerland*
[b] *Hexcel Reinforcements, Les Aveniers, France*
[c] *Département Technologie des Polymères et Composites & Ingénierie Mécanique, École des Mines de Douai, France*
[d] *Laboratoire Ondes et Milieux Complexes, Université du Havre, France*
[e] *Chaire sur les Composites à Haute Performance, École Polytechnique de Montréal, Canada*
[f] *Division of Materials, Mechanics & Structures, University of Nottingham, UK*
[g] *Department of Metallurgy and Materials Engineering, Katholieke Universiteit Leuven, Belgium*
[h] *Deutsches Zentrum für Luft- und Raumfahrt at AIRBUS Operations GmbH Bremen, Germany*
[i] *Institut für Polymerwerkstoffe und Kunststofftechnik, Technische Universität Clausthal, Germany*
[j] *Department of Composite Materials and Structures, ONERA, France*
[k] *Laboratoire de Technologie des Composites et Polymères, École Polytechnique Fédérale de Lausanne, Switzerland*
[l] *Department of Mechanics of Materials and Constructions, Vrije Universiteit Brussel, Belgium*

In this international permeability benchmark exercise, in-plane permeability data for two reinforcement fabrics, obtained using a total of 16 different experimental procedures, were compared. Although, for each procedure, the results appear consistent, different procedures result in a scatter of up to one order of magnitude in principal permeability values for each fabric at any given fibre volume fraction. The ratio of the principal permeability values varies by factors of up to 2. While experimental uncertainties and variability of the specimens affect the scatter in results for any single series of experiments, it is sus-pected that the main source of scatter in results from different procedures is related to human factors. Aiming at standardisation of measurement methods and interchangeability of results, "good practice" guidelines will be formulated in order to eliminate sources of scatter.

1. Introduction

In Liquid Composites Moulding (LCM) processes, a textile reinforcement structure is preformed to the geometrical shape of the component to be produced. The dry preform is inserted into a mould cavity. After closing of the mould, liquid resin is injected. Once the preform is impregnated and the resin is cured, the component is demoulded and can be finished. Its quality is determined by the quality of impregnation of the reinforcement and the degree of cure of the thermoset matrix material. The cure characteristics of the matrix depend on the resin chemistry and will not be discussed here. The impregnation of the textile preform with resin is typically described using the model of a viscous liquid flowing through a (homogeneous) porous medium. Darcy's law [1], which is frequently formulated as

$$\mathbf{v} = -\frac{\mathbf{K}}{\eta}\nabla p, \tag{1}$$

states a dependence of the phase-averaged (resin + fibres) flow velocity, $\mathbf{v}$, on the permeability of the textile material, $\mathbf{K}$, the viscosity of the resin, η, and the gradient of the pore-averaged pressure inside the mould, ∇p. Based on Eq. (1), the process parameters for production of composite components applying LCM-technology (e.g. location of injection gates and vents in the mould) can be optimised to achieve complete impregnation, i.e. high quality, of the finished components, and the cycle time can be predicted.

The permeability of fibrous structures is generally anisotropic and can be described by a second order tensor. For the simplest case of aligned filaments, various models [2–5] describe the axial and transverse permeability as a function of fibre volume fraction, filament radius and geometrical constants. The geometrical constants in the models, and thus the absolute permeability values, can be estimated predictively only for idealised basic cases of uniformly distributed filaments, which allow simplifying approximations to be made for the flow [3,4].

* Corresponding author.
E-mail address: andreas.endruweit@nottingham.ac.uk (A. Endruweit).

The permeability of textile fabrics is typically determined by homogenisation of the properties of fibre bundles and inter-bundle gaps, which form a (in some cases geometrically highly complex) dual-scale pore network. Since the orientation of the principal flow directions is determined by the pore configuration (i.e. the fibre orientations), for thin two-dimensional fabrics, the first two principal axes can be assumed to lie in the fabric plane, while the third axis can be assumed to be oriented perpendicular to the fabric plane. However, it can be argued that this is not necessarily the case for fibrous preforms in general [6]. A significant body of work has been published on modelling the permeability of reinforcement fabrics with specific architectures, in particular addressing the problem of dual-scale porosity (a few recent examples are given in [7–9]). A general problem is that the permeability of a bundle of non-uniformly distributed filaments and the geometry of the inter-bundle gaps and their contribution to the fabric permeability are hard to describe accurately. Thus, fabric permeability models describe typically the dependence on the fibre volume fraction, which are of most interest for many practical applications, but cannot predict quantitatively any constants related to the geometry of the complex pore network. These can only be determined directly from permeability measurement (as, e.g., in [9]) or, alternatively, based on advanced numerical methods, e.g. virtual experiments via flow simulations [10], which require detailed input from experimental pore geometry characterisation.

With permeability measurement being of major importance for characterisation of textile impregnation, not only in the field of composites processing, standards have been established for measurement of the through-thickness permeability of clothing and technical textiles (ASTM D737: air flow; ISO 15496: water vapour flow) and compressed geotextiles (ASTM D5493: water flow). To characterise resin flow in reinforcement textiles, a wide variety of experimental methods for permeability measurement has been developed [11]. Most address measurement of the in-plane permeability, which is of high relevance to LCM, since composites are most frequently processed in thin shell-like structures. However, there is a complete lack of standardisation for measurement of the in-plane permeability of fabrics, and it is well known that permeability data obtained using different methods are not necessarily consistent. In 1995, Parnas et al. [12] proposed use of a reference fabric for standardisation of permeability measurement methods, but to date no standards or guidelines have been put in place. Lundström et al. [13] report on a small-scale benchmark exercise, in which issues of repeatability and reproducibility of permeability measurement were addressed. For a reference material, the scatter of results obtained by different laboratories was in the same order of magnitude as the experimental uncertainty. However, there were only three participants, who all used the same set-up and were trained before carrying out the experiments. Thus, the observed scatter was attributed to differences in specimen preparation.

The international permeability benchmark exercise documented here was initiated by ONERA (Office National d'Études et de Recherches Aérospatiales, France) and Katholieke Universiteit Leuven. As a first step towards standardisation of permeability measurement, the aim was to get an overview of the methods in practical use and the range of results obtained implementing these methods. Twenty institutions and industrial end users from 12 countries replied to a first invitation to participate. For the two reinforcement textiles discussed in this report (Table 1), a 2×2 twill weave carbon fibre fabric (G0986) and a 2×2 twill weave E-glass fibre fabric (01113), both provided by HEXCEL, 11 participants (Table 2) submitted measured in-plane permeability data (for either one or both materials). Participants were instructed to measure the permeability at a target fibre volume fraction of 50% or as close as possible to this value, and were then left to implement their own procedures and protocols. Feedback on procedures and results was provided to all participants in round table discussions at the Flow Processes in Composite Materials conferences in Montréal (FPCM 9, 2008) and Ascona (FPCM 10, 2010).

2. Permeability measurement

2.1. General considerations

A variety of experimental methods for determination of the fabric permeability has been developed. They can be distinguished based on three main criteria:

- flow geometry (linear/radial),
- injection boundary condition (constant pressure/constant flow rate),
- saturation state of the fabric specimen (saturated/unsaturated).

While a more complete review of methods for permeability measurement is given in a recent paper by Sharma and Siginer [11], the basic principles of frequently implemented methods will be discussed in the following.

For unsaturated linear flow at constant injection pressure, the permeability is determined from injection experiments in a rectangular flow channel with a linear injection gate, which needs to be realised such that the fluid penetrates all layers of the specimen equally. The flow front is assumed to be straight and oriented perpendicular to the flow channel axis. Time integration of Darcy's law gives the permeability along the flow direction,

$$K = -\frac{x_{ff}^2 \Phi \eta}{2\Delta p t_{ff}}. \tag{2}$$

Here x_{ff} is the flow front position at an injection time t_{ff}, Δp is the pressure difference between injection pressure and ambient pressure (i.e. gauge pressure), η is the viscosity of the injected fluid, and Φ is the porosity of the fabric specimen. Issues of fibre wetting and its influence on Δp and the determination of K will be discussed below. Inclusion of the factor Φ results from the difference between the flow front velocity in unsaturated flow (corresponding to the average flow velocity of the fluid molecules along the applied pressure gradient) and the velocity defined in Darcy's law. The porosity of a specimen is related to the fibre volume fraction V_f via

$$\Phi = 1 - V_f. \tag{3}$$

In practice, V_f can be determined from

$$V_f = \frac{nS_0}{\rho_f h}, \tag{4}$$

where n is the number of fabric layers in the specimen, S_0 is the superficial density of the fabric, ρ_f is the density of the fibre material, and h is the cavity height. The flow front position as a function of injection time, $x_{ff}(t_{ff})$, is most frequently determined by visual monitoring through the transparent top of the flow channel [14,15]. Alternative approaches for flow front tracking are use of fibre optic sensors [16], thermistors [17], pressure transducers [18] or ultrasound and electrical resistance measurements [19]. Concurrent data reduction schemes for the acquired $x_{ff}(t_{ff})$ raw data are discussed by Ferland et al. [20].

For saturated linear flow, Darcy's law can directly be solved for the permeability

$$K = -\frac{Q\eta L}{A\Delta p}, \tag{5}$$

where Q is the flow rate, A is the flow channel cross-sectional area, and L is the specimen length. In the case of constant injection

Table 1
Properties of fabrics characterised in this study.

Fabric	01113 1000 TF970	G0986 D 1200
Architecture	Twill 2 × 2	Twill 2 × 2
Nominal superficial density (g/m^2)	390	285
Nominal construction	Warp: 5.9 yarns/cm Weft: 6.6 yarns/cm	Warp: 3.5 yarns/cm Weft: 3.5 yarns/cm
Weight distribution	Warp: 53% Weft: 47%	Warp: 50% Weft: 50%
Yarns warp	E-glass	Carbon HT
Type	(EC9 68) × 5	HTA 5131 6K
Nominal filament diameter (μm)	9	7
Nominal linear density (tex)	340	400
Yarns weft	E-glass	Carbon HT
Type	(EC9 136) × 2	HTA 5131 6K
Nominal filament diameter (μm)	9	7
Nominal linear density (tex)	272	400

Table 2
Participants in benchmark exercise.

Institution	Division	Country	Referred to as
Vrije Universiteit Brussel	Department of Mechanics of Materials and Constructions	Belgium	Brussels
Technische Universität Clausthal	Institut für Polymerwerkstoffe und Kunststofftechnik	Germany	Clausthal
Deutsches Zentrum für Luft- und Raumfahrt at AIRBUS Operations GmbH Bremen		Germany	DLR
École des Mines de Douai	Département Technologie des Polymères et Composites & Ingénierie Mécanique	France	Douai
Université du Havre	Laboratoire Ondes et Milieux Complexes	France	le Havre
École Polytechnique Fédérale de Lausanne	Laboratoire de Technologie des Composites et Polymères	Switzerland	Lausanne
Katholieke Universiteit Leuven	Department of Metallurgy and Materials Engineering	Belgium	Leuven
École Polytechnique de Montréal	Chaire sur les Composites à Haute Performance	Canada	Montréal
University of Nottingham	Division of Materials, Mechanics & Structures	United Kingdom	Nottingham
Office National d'Études et de Recherches Aérospatiales	Department of Composite Materials and Structures	France	ONERA
Eidgenössische Technische Hochschule Zürich	Centre of Structure Technologies	Switzerland	Zürich

pressure, the flow rate can be determined from the mass flow (measured by weighing of the fluid mass that has passed through the specimen as a function of injection time) and the fluid density [21]. In the case of constant injection flow rate, the pressure gradient along the specimen (which is constant) can be measured. Experiments of this type can be used for measurement of in-plane or through-thickness permeability.

The radial penetration of liquids into planar porous media has been extensively discussed in the literature, notably by Adams and Rebenfeld [22,23]. Unsaturated radial flow is governed by the Laplace-equation, which is derived from combination of Darcy's law with the equation of continuity for incompressible fluids. Solution of the problem for constant injection pressure and isotropic fabric gives the permeability

$$K = \frac{\Phi\eta R_0^2}{4\Delta p t_{ff}} \left(\frac{R_{ff}}{R_0}\right)^2 \left(2\ln\left(\frac{R_{ff}}{R_0}\right) - 1\right) + 1\Bigg), \tag{6}$$

where R_{ff} is the radius of the circular flow front at time t_{ff}, and R_0 is the radius of the circular injection gate.

The general case of anisotropic fabrics with elliptical flow fronts is more complex. Formulation of the problem in elliptical co-ordinates [24] allows an equation similar to Eq. (6) to be derived for the equivalent isotropic permeability. Determination of the principal permeability values K_1 and K_2 from the equivalent isotropic permeability is based on measurement of the axes R_1 and R_2 of the flow front ellipse as a function of time. This method was extended by Weitzenböck et al. [25,26] to determine the permeability without prior knowledge of the orientation of the principal axes.

Radial flow experiments at constant injection flow rate [27,28] allow permeability measurement at constant pressure gradient. For saturated flow and isotropic fabric, the permeability can be derived from

$$K = \frac{Q\eta}{2\pi h\Delta p} \ln\left(\frac{R_{ff}}{R_0}\right). \tag{7}$$

Based on the same concept, Han et al. [29] presented a method for characterisation of anisotropic fabrics, in which the pressure gradient is measured in different directions. For all radial injection techniques, a circular injection gate (defining R_0) needs to be cut out of the specimens, such that pure in-plane flow can develop.

It is debatable, which method is to be preferred. Comparison of experimental methods for determination of the in-plane principal permeability values based on visual tracking of the flow front propagation [13,30,31] suggests that separate measurement of K_1 and K_2 in unsaturated linear flow experiments shows the highest reproducibility. Results from radial flow experiments are in general consistent with results from linear flow experiments, but tend to show higher variations. However, if the orientation of the principal permeability axes is unknown, both in-plane principal permeability values and the orientation of the principal permeability axes can be determined in one radial flow experiment [25,26], while three linear flow experiments (along different fabric directions) are required [32].

In addition, linear flow experiments are inherently susceptible to errors in the measured permeability induced if the principal fabric axis does not coincide with the flow channel axis. In this case, a transverse component of the fluid flow occurs, violating the assumption of purely uni-directional flow in Eqs. (2) and (5). This effect is most severe at an angle of 45° between principal permeability direction and flow channel axis, small flow channel aspect ratio and high reinforcement ratio of anisotropy. To minimise the

induced error, the aspect ratio of the flow channel (length/width) should be greater than the ratio of anisotropy of the reinforcement [15,33].

It is also well known that linear flow experiments can be affected by racetracking along the specimen edges [34]. This is caused by (unavoidable) gaps between specimen edges and cavity walls and can result in increased average flow front velocity or increased flow rate, thus leading to overestimation of the permeability. The effect can be mitigated by sealing of the specimen edges, although this can create new issues (e.g. uncertainties regarding the effective channel width). Procedures have also been proposed to eliminate racetracking by physically separating fluid flowing through gaps along the edges and through the specimen (in saturated flow) [35], or to correct permeability values measured in the presence of racetracking based on factors derived from the observed flow front patterns (in unsaturated flow) [36].

To obtain reliable in-plane permeability data, Wang et al. [37] recommended evaluation of both linear and radial flow experiments.

Permeability values determined in unsaturated and saturated flow experiments may differ because of the occurrence of transient capillary effects in unsaturated flow as documented, e.g., in an overview given by Pillai [38]. Wetting of dry fibres in unsaturated flow is affected by the capillary pressure, which is given by the surface tension of the fluid, the contact angle at the fluid-fibre-interface (which is affected by surface treatment of the fibres [39]) and the hydraulic radius of the fibres [40]. This results in a difference between applied and effective flow-driving pressure gradient. Since it is not possible to determine this difference in actual injection situations, the concept of unsaturated permeability, in which geometrical drag and capillary effects are combined, was introduced. This is typically different from saturated permeability, which describes geometrical drag only. It could be argued that Darcy's law was originally derived for saturated flow and thus, the permeability should only be determined in saturated flow experiments. On the other hand, the conditions during impregnation of dry fabrics in LCM processes are generally thought to be reproduced well in unsaturated flow experiments.

2.2. Procedures in this study

The main characteristics of the experimental procedures implemented by the participants are listed in Table 3. More detailed information on some of the procedures is given in the references [18,41–48]. Since 5 out of the 11 participants implemented more than one method, a total of 16 different procedures are listed. All are derived from the concepts formulated in Eqs. (2), (5), (6), and (7), with the exception of the through-thickness compression method implemented by Douai, which is described in detail by Comas-Cardona et al. [42]. Referring to the three main criteria for distinction of the methods, the table can be summarised as follows:

- 9 linear/7 radial injection geometries;
- 12 constant pressure/3 constant flow rate boundary conditions; 1 other;
- 9 saturated/7 unsaturated flow experiments.

Table 3
Main characteristics of experimental procedures for permeability measurement implemented by the participants.

Institution	Linear/radial injection	Saturated/ unsaturated flow	Test fluid	Const. pressure/const. flow rate injection	Exp. strategy	Exp. technique	Reference
Brussels	Radial	Unsaturated	Corn syrup	Const. pressure	Flow front tracking	Array of electrical sensors	Hoes et al. [41]
Clausthal	Linear	Saturated	Vegetable oil	Const. pressure	Measure mass flow	Collect fluid per time unit	
Clausthal	Linear	Unsaturated	Vegetable oil	Const. pressure	Flow front tracking	Visual	
DLR	Radial	Saturated	Vegetable oil	Const. flow rate	Measure pressure field	Array of pressure sensors	
DLR	Radial	Unsaturated	Vegetable oil	Const. flow rate	Measure pressure field	Array of pressure sensors	
Douai	Linear	Saturated	Di octyle phtalate	Const. pressure	Measure mass flow	Collect fluid per time unit	
Douai	Radial, through-thickness compression	Saturated	Silicon oil	Const. compression speed	Measure pressure field	Pressure sensors	Comas-Cardona et al. [42]
le Havre	Linear	Saturated	Silicon oil	Const. pressure	Measure mass flow	Collect fluid per time unit	
le Havre	Linear	Unsaturated	Silicon oil	Const. pressure	Flow front tracking	Visual	
Lausanne	Linear	Saturated	Polyethylene glycol/water	Const. pressure	Measure mass flow	Collect fluid per time unit	Verrey [43]
Leuven	Radial	Unsaturated	Polyol (polyurethane)	Const. pressure	Flow front tracking	Visual	Gommer [44,45]
Montréal	Linear	Saturated	Silicon oil	Const. flow rate	Measure pressure difference	Pressure sensors	
Montréal	Linear	Unsaturated	Silicon oil	Const. pressure	Flow front tracking	Visual	Demaria et al. [46]
Nottingham	Radial	Unsaturated	Engine oil	Const. pressure	Flow front tracking	Array of pressure sensors	Endruweit et al. [18]
ONERA	Linear	Saturated	Silicon oil	Const. pressure	Measure mass flow	Collect fluid per time unit	Laine et al. [47]
Zürich	Radial	Saturated	Silicon oil	Const. pressure	Measure pressure field	Array of pressure sensors	Arbter [48]

All participants used test fluids instead of resin, which are easier to handle since they do not cure and have the advantage of constant viscosity at constant injection conditions. In 12 cases, oil (different types, viscosities) was used, in 4 cases, other fluids.

The measured (apparent) fabric permeability reflects the actual permeability and, in addition, is affected by the viscosity of the test fluid and the injection pressure and/or flow rate. The actual permeability depends strongly on the porosity (i.e. fibre volume fraction) [2–5], which, according to Eq. (4), is given by the number of fabric layers and the cavity height. Because of these dependencies, tool design, which affects the effective cavity height, and determination of viscosity and injection pressure/flow rate are subject to further scrutiny. Details on the experimental procedures are listed in Tables 4–6. Blank cells in the tables reflect the varying level of detail provided by the participants.

Regarding the tool design (Table 4), the cavity/specimen size should be large compared to the dimensions of the textile unit cell, since permeability measurement implies homogenisation of micro- and meso-scale flow effects. For radial flow experiments, the radius R_0 in Eqs. (6) and (7) is typically identified with the radius of a circular hole cut in the preform at the injection gate, where the injection pressure is measured. If no hole is cut in the preform, the effective value of R_0, which in this case is affected by through-thickness flow effects, and the effective pressure at this radius are unknown and are not necessarily well approximated by the radius of the inlet hole in the mould. This may have a significant influence on the results. It is also well known that for anisotropic material, the flow front shape (and pressure field) near the injection gate are influenced by the circular shape of the inlet, and an elliptical flow front will only develop in a certain distance from the injection gate. To avoid measurement of the influence of the injection gate rather than the effect of the fabric structure on fluid flow, R_0 should generally be small compared to the specimen size.

A significant problem is that the actual cavity height may not be identical to the assumed height. Increased cavity height h results in decreased V_f according to Eq. (4), and thus in an increase in actual permeability. This is related to tool deflection, which may be caused by reaction forces exerted by the compacted fabric specimen and by the fluid pressure inside the cavity. The deflection depends on the stiffness, i.e. material and geometry, of the tool. It can be significant, in particular if a transparent mould top from polymethylmethacrylate (PMMA) with relatively low modulus is used to allow visual flow front tracking. Methods, which do not require visual flow front tracking through a transparent mould top, allow use of materials with higher modulus (typically metals) and thus tend to be less affected by tool deflection. In these cases, flow front tracking or measurement of pressure fields is sensor-based, which can imply new limitations. For example, Hoes et al. [41] pointed out that application of their technique (electrical sensors) is limited to non-conductive reinforcements and conductive test fluids. Regardless of the tool material, additional stiffening structures are frequently used to minimise deflections. A related issue is incomplete closing of the mould, which may occur at high V_f and result in increased permeability.

Regarding determination of the fluid viscosity (Table 5), a frequently adopted procedure is acquisition of a viscosity–temperature curve for the test fluid and measurement of the test fluid temperature prior to or during the injection experiment. However, since the fluid is dispersed in microscopic pores in the specimen, the effective amount of fluid in contact with the tool or the fibres is small, and it is susceptible to changes in temperature and viscosity. Thus, it is crucial that the mould tool and the fabric specimen have the same temperature as the fluid to avoid changes in viscosity during injection. Some participants characterised the viscosity of their test fluid as a function of shear rate. Most found Newtonian behaviour for the range of shear rates considered relevant here.

Table 4
Details on tool set-up and deflection.

Institution	Specimen dimensions	Cavity height adjustment	Tool material	Closing mechanism	Closing/deflection controlled or monitored
Brussels	300 mm × 300 mm, 6 mm dia. inj. gate	Spacer rods	Steel plates, 13 mm	Hydraulic	Closing force 40 kN
Clausthal (01113)	240 mm × 400 mm	Spacer frames	Steel, 60 mm (bottom) Glass, 70 mm (top)	Manual	Deflection quantified as <0.15 mm
Clausthal (G0986)	200 mm × 300 mm	Spacer frames	Glass, 12 mm + polycarbonate, 10 mm + steel stiffening structure (top and bottom)	Manual	Thickness variation <0.04 mm measured for moulded and cured plates (inj. pressure 3×10^5 Pa)
DLR	600 mm × 600 mm			Hydraulic	
Douai (linear sat.)	300 mm × 180 mm	Spacer rods	Steel (bottom), PMMA (top) + steel stiffening bars	Manual	Deflection quantified as <0.1 mm at inj. gate
Douai (through-thickness compression)	Circular, 135 mm diameter	Displacement controlled (materials testing machine)	Compression platens Aluminium (bottom) Steel (top)	Power screw drive	Uncertainty in height depends on accuracy of testing machine
le Havre	100 mm × 400 mm 100 mm × 500 mm		Steel, 20 mm (bottom) Glass, 40 mm (top)	Manual	Direct contact measurement of cavity height
Lausanne	80 mm × 120 mm		Steel, 25 mm (bottom) PMMA, 25 mm (top)	Manual	Uncertainty in actual cavity height quantified as ±0.1 mm
Leuven	300 mm × 500 mm, no hole at inj. gate	Spacer frames	Aluminium (bottom) PMMA, 50 mm (top) + steel stiffening structure	Manual	Actual cavity height distribution quantified, variation <0.15 mm
Montréal	100 mm × 400 mm	Spacer frames	Aluminium (bottom), Glass (top) + steel stiffening structure	Pneumatic	
Nottingham	Circular, 400 mm diameter, 10 mm dia. inj. gate	Spacer frames	Aluminium, 25 mm + steel stiffening structure (top and bottom)	Manual	Deflection quantified as <0.1 mm (dial gauge)
ONERA	120 mm × 500 mm	Spacer frames	Steel, 50 mm (bottom) Glass, 30 mm (top) + steel stiffening structure		Cavity height distribution quantified, variation 0.01 mm . . . 0.02 mm
Zürich	380 mm × 380 mm, 50 mm dia. inj. gate	Compaction pressure controlled		Pneumatic	Actual cavity height measured using laser-displacement meter

Table 5
Details on test fluid viscosity.

Institution	Test fluid	Determination of viscosity	Temperature (°C)	Viscosity (Pa s)	Temperature control	Additional comments
Brussels	Corn syrup	Measured before injection	21.1 ... 21.6	0.107 ... 0.115		
Clausthal	Vegetable oil	From $\eta(T)$ curve, T measured before each experiment	19 ... 21	0.066 ... 0.071	Test fluid and set-up stored at identical temperature	
DLR	Vegetable oil		20	0.090		
Douai (linear sat.)	Di octyle phthalate	From $\eta(T)$ curve, T measured before each experiment	17 ... 18	0.119 ... 0.128	Test fluid and set-up stored at identical temperature	Newtonian behaviour stated
Douai (1D compression)	Silicon oil	From $\eta(T)$ curve, T measured before each experiment	17 ... 18	0.1 ... 10 (different grades)	Test fluid and set-up stored at identical temperature	Newtonian behaviour stated
le Havre	Silicon oil	From $\eta(T)$ curve, T measured before each experiment	20	0.107	Test fluid and set-up stored at identical temperature	Newtonian behaviour verified for $T = 20$ °C
Lausanne	Polyethylene glycol/water	Measured before injection	18 ... 24	0.026 ... 0.027	Test fluid and set-up stored at identical temperature	Newtonian behaviour verified
Leuven	Polyol (polyurethane)	From $\eta(T)$ curve, T measured during each experiment	22	0.067	Test fluid and set-up stored at identical temperature	Fluid shear thinning (at $T = 22$ °C)
Montréal	Silicon oil	From $\eta(T)$ curve, T measured during each experiment	23		Test fluid and set-up stored at identical temperature	Newtonian behaviour verified
Nottingham	Engine oil	From $\eta(T)$ curve, T measured before experiment	21 ... 22	0.260 ... 0.270	Test fluid and set-up stored at identical temperature	
ONERA	Silicon oil	From $\eta(T)$ curve, T measured during each experiment			Test fluid and set-up stored at identical temperature	Newtonian behaviour stated
Zürich	Silicon oil	Measured at given T	23	0.105		

Table 6
Details on test fluid injection.

Institution	Injection pressure/flow rate control	Method for monitoring	Pressure difference (10^5 Pa)	Flow rate (10^{-6} m^3/s)
Brussels	Pressure pot injection unit	Pressure measured at injection gate	1	
Clausthal	Pressure pot	Pressure measured at pressure pot	1	
DLR	Injection station	Pressure measured at injection gate		1.33 (01113) 1.67 (G0986)
Douai (linear sat.)	Pressure pot injection unit	Pressure measured at inlet and outlet	2.4 ... 2.8 (01113) 2.0 ... 2.1 (G0986)	0.05 ... 0.16 (01113) 0.17 ... 0.18 (G0986)
le Havre				
Lausanne	Pressure pot injection unit	Pressure measured at injection gate	0.35 ... 1.3 (01113) 0.38 ... 1.1 (G0986)	
Leuven	Pressure pot at injection gate + vacuum pump at vent	Pressure measured at pressure pot, vacuum measured at outlet	1.2	
Montréal	Pressure pot		1.15 ... 3.10 (01113) 0.65 ... 3.20 (G0986)	
Nottingham	Pressure pot	Pressure measured at injection gate	3.55 ... 3.73 (01113) 3.52 ... 3.65 (G0986)	
ONERA	Pressure pot	Pressure measured at inlet and outlet	0.1 ... 6.0	
Zürich	Pressure pot	Pressure measured at pressure pot	0.35, 1.08, 1.80	

Leuven found shear-thinning of their test fluid and applied a correction procedure for the measured permeability values. This implied obtaining a curve for the shear rate dependence of the test fluid viscosity, estimation of an average shear rate for flow in the experiments, and correction of the apparent fluid viscosity [44].

For complete characterisation of the test fluid, Clausthal quote a value for the surface tension. However, for determination of the wetting behaviour, contact angle and hydraulic fibre radius need to be known as well.

The information in Table 6 indicates that, due to its simplicity, injections at constant pressure are most frequently realised using a pressure pot set-up. For accurate determination of Δp, the pressure should be measured at the injection gate rather than at the pressure pot, since pressure drop in the tubes (which increases with decreasing tube diameter and increasing tube length) can cause uncertainty. The accuracy of pressure measurement should be quantified to allow estimation of experimental errors as will be discussed in Section 3.1. Equally, the accuracy of the pump should be quantified, if the fluid is injected at constant flow rate. In-plane permeability measurement in unsaturated flow experiments at constant injection flow rate (radial or linear) may also be affected by transient differences between actual and prescribed flow rate. During impregnation, the volume of permeated fabric increases, resulting in increased flow resistance and thus a pressure increase in the pumping system. This may cause accidentally entrapped residual gas to be compressed or compliant components of the system (e.g. rubber tubes) to be expanded, thus causing a reduction of the actual flow rate. When the pressure increases further, the whole system becomes stiffer. Thus, the flow rate increases again, eventually converging to the prescribed value. To avoid underestimation of the permeability due to this effect, the fluid duct system needs to be designed sufficiently stiff, and entrapment of gas bubbles needs to be avoided. It is to be noted that a steady flow rate is expected to evolve for saturated flow.

It was recommended to all participants that, if they have not already done so, procedures should be put in place to monitor and control tool deflection, test fluid viscosity and injection pressure/flow rate, and known issues should be documented.

3. Results and discussion

3.1. General comments

Results for the measured permeability of both fabrics are summarised in Tables 7 (G0986) and 8 (01113). The angle θ is defined as the angle between the fabric weft direction and the principal flow direction, i.e. the major axis of the elliptical flow front in case of radial flow. If the weft or warp direction were identified as main flow direction, these were converted into values of θ, i.e. 0° or 90° respectively. Where available (and appropriate), average value, standard deviation and coefficient of variation (standard deviation/average) are given. In some cases, average and standard deviation were calculated, even if, strictly speaking, statistical evaluation of the data is questionable, i.e. if only two values were available in a series. Since permeability data typically show considerable variability (as will be discussed below), quoted values should be based on series of experiments with numbers of repeats high enough to give confidence in the results. Standard deviation or coefficient of variation should be quoted in addition to average values.

Typically, permeability values are quoted at given fibre volume fractions. However, Zürich acquired a set of original data over a range of fibre volume fractions (between 0.48 and 0.70 for G0986 and between 0.49 and 0.64 for 01113) for the weft and warp direction of each fabric. From these, the constants in the equations in Tables 7 and 8, which are derived from the Kozeny–Carman relation [2], were determined by curve fitting. Based on these constants, calculation of permeabilities at arbitrary fibre volume fractions was suggested. The quality of the fit of the Kozeny–Carman model to the original data, and thus the confidence in this procedure, was found to be higher for 01113 than for G0986. Nottingham quote a coefficient of variation of 0% for V_f (both fabrics). This reflects the small effect of local variability in the fabric structure on the mass of the relatively large specimens (determined by weighing), but does not take potential differences between assumed and actual values of h into account.

It is to be noted that some of those participants, who carried out linear flow experiments, measured the permeability along two fabric directions, weft and warp. For the fabrics characterised in this study, this is sufficient since the principal permeability axes coincide with the weft and warp directions, as demonstrated by other participants. However, full characterisation of the in-plane permeability tensor generally requires measurement along three fabric directions (as demonstrated by Montréal), if linear flow experiments are used [32]. Some participants even determined the permeability along one fabric direction only. While this would fully characterise isotropic material, it is not sufficient here, since the values for K_1/K_2 indicate a significant degree of anisotropy. As discussed above, the specimen aspect ratio should be greater than K_1/K_2 for linear injections. This implies that for some of the documented experiments, the accuracy may have been compromised, in particular for 01113 (minimum specimen aspect ratio was 1.5).

To provide an overview of all data and allow easy comparison, the principal permeability values K_1 and K_2 and the ratio K_1/K_2 as

Table 7
Results for G0986: a short characterisation of the experimental method, number of repeats N_{exp}, cavity height h, number of layers n, fibre volume fraction V_f, principal permeability values, K_1 and K_2, angle θ characterising the principal flow direction, and ratio K_1/K_2 are listed; average value, standard deviation and coefficient of variation (standard deviation/average) are given, where appropriate. Not all data points submitted by Douai (1D compression method) are listed.

Institution	Method	N_{exp}	h (mm)	n	V_f	K_1 (10^{-10} m^2)	K_2 (10^{-10} m^2)	θ	K_1/K_2
Clausthal	Linear sat.	2 (weft) 2 (warp)	5	16	0.51	0.341 ± 0.028 (±8%)	0.247 ± 0.017 (±7%)	0°	1.381 ± 0.149 (±11%)
Clausthal	Linear unsat.	2 (weft) 2 (warp)	5	16	0.51	0.287 ± 0.017 (±6%)	0.210 ± 0.014 (±7%)	0°	1.367 ± 0.121 (±9%)
DLR	Radial sat.		3.8	12	0.51	0.476	0.365	0°	1.304
DLR	Radial unsat.		3.8	12	0.51	0.479	0.374	0°	1.281
Douai	Linear sat.	3	2	6	0.49	0.833 ± 0.066 (±8%) weft only			
Douai	Radial sat., 1D compression	9	1.6 . . . 2.7	6	0.42	2.1 ± 0.36 (±17%)			
Douai	Radial sat., 1D compression	9	1.6 . . . 2.7	6	0.45	1.3 ± 0.23 (±18%)			
Douai	Radial sat., 1D compression	9	1.6 . . . 2.7	6	0.48	0.79 ± 0.12 (±15%)			
Douai	Radial sat., 1D compression	9	1.6 . . . 2.7	6	0.51	0.42 ± 0.061 (±15%)			
Douai	Radial sat., 1D compression	9	1.6 . . . 2.7	6	0.56	0.19 ± 0.028 (±15%)			
le Havre	Linear unsat.	1 (weft) 1 (warp)	3.7	11	0.47	1.153	0.831	0°	1.387
le Havre	Linear unsat.	1 (weft) 1 (warp)	3.7	12	0.52	0.528	0.496	0°	1.065
le Havre	Linear unsat.	1 (weft) 1 (warp)	3.7	13	0.56	0.368	0.198	0°	1.859
Lausanne	Linear sat.	3	3.0		0.50	5.39 ± 0.64 (±12%) warp only			
Montréal	Linear sat.	2	3.1	9	0.46	5.395 ± 2.892 (±54%) warp only			
Montréal	Linear unsat. Scheme 1	43 (three directions)	3.1	9	0.46	4.233	2.134	22°	1.984
Montréal	Linear unsat. Scheme 2	43 (three directions)	3.1	9	0.46	4.323	2.130	22°	2.030
Nottingham	Radial unsat.	20	2	6	0.49 ± 0.00 (±0%)	3.232 ± 0.936 (±29%)	1.720 ± 0.463 (±27%)	−3° ± 8°	1.879 ± 0.743 (±40%)
ONERA	Linear sat.	10		1	0.54	0.450 ± 0.043 (±10%) warp only			
ONERA	Linear sat.	10		2	0.54	0.287 ± 0.090 (±31%) warp only			
ONERA	Linear sat.	3		8	0.54	0.153 ± 0.097 (±63%) warp only			
Zürich	Radial sat.	75		5		$14.5 \times (1 - V_f)^3/V_f^2$ (±32%)	$5.53 \times (1 - V_f)^3/V_f^2$ (±32%)	13° ± 6°	2.64 ± 0.28 (±11%)

Table 8
Results for 01113: a short characterisation of the experimental method, number of repeats N_{exp}, cavity height h, number of layers n, fibre volume fraction V_f, principal permeability values, K_1 and K_2, angle θ characterising the principal flow direction, and ratio K_1/K_2 are listed; average value, standard deviation and coefficient of variation (standard deviation/average) are given, where appropriate. Not all data points submitted by le Havre are listed.

Institution	Method	N_{exp}	h (mm)	n	V_f	K_1 (10^{-10} m^2)	K_2 (10^{-10} m^2)	θ	K_1/K_2
Brussels	Radial unsat.	30	3	10	0.5	0.354 ± 0.041 (±12%)	0.083 ± 0.009 (±11%)		4.296 ± 0.677 (±16%)
Clausthal	Linear unsat.	6 (weft) 6 (warp)	4.7	16	0.51	0.202 ± 0.015 (±8%)	0.063 ± 0.006 (±10%)	90°	3.206 ± 0.389 (±12%)
DLR	Radial sat.		4.2	14	0.50	1.040	0.612	90°	1.699
DLR	Radial unsat.		4.2	14	0.50	1.020	0.485	90°	2.103
Douai	Linear sat.	3 (weft) 3 (warp)	2	6	0.46	0.586 ± 0.034 (±6%)	0.224 ± 0.028 (±13%)	90°	2.616 ± 0.362 (±14%)
le Havre	Linear sat.	1 (weft) 1 (warp)	3.7	11	0.45	0.560	0.292	90°	1.918
le Havre	Linear sat.	2	3.7	12	0.51	0.325 ± 0.007 (±2%) warp only			
le Havre	Linear sat.	1	3.7	13	0.55	0.180 warp only			
le Havre	Linear unsat.	1 (weft) 1 (warp)	3.7	11	0.45	0.417	0.138	90°	3.022
le Havre	Linear unsat.	2	3.7	12	0.51	0.226 ± 0.037 (±16%) warp only			
le Havre	Linear unsat.	1	3.7	13	0.55	0.127 warp only			
le Havre	Linear unsat.	1	3.7	14	0.58	0.079 warp only			
Lausanne	Linear sat.	3	3.9		0.50	4.45 ± 0.45 (±10%) warp only			
Leuven	Radial unsat.	5	1.49	4	0.41	2.010 ± 0.387 (±19%)	0.477 ± 0.145 (±30%)		4.214 ± 1.516 (±36%)
Leuven	Radial unsat.	6	1.49	5	0.51	0.443 ± 0.163 (±37%)	0.109 ± 0.032 (±30%)		4.064 ± 1.922 (±47%)
Leuven	Radial unsat.	4	1.66	6	0.54	0.306 ± 0.016 (±5%)	0.077 ± 0.002 (±2%)		3.995 ± 0.234 (±6%)
Montréal	Linear unsat. Scheme 1	11 (3 directions)	3.1	10	0.49	0.911	0.316	90°	2.889
Montréal	Linear unsat. Scheme 2	11 (3 directions)	3.1	10	0.49	1.152	0.305	105°	3.777
Nottingham	Radial unsat.	17	2	7	0.53 ± 0.00 (±0%)	0.628 ± 0.096 (±15%)	0.340 ± 0.062 (±18%)	95° ± 7°	1.847 ± 0.440 (±24%)
Zürich	Radial sat.	44		8		$2.86 \times (1\text{-}V_f)^3/V_f^2$ (±11%)	$0.818 \times (1\text{-}V_f)^3/V_f^2$ (±17%)	95° ± 2°	3.65 ± 0.59 (±16%)

functions of the fibre volume fraction V_f are plotted in Figs. 1–6[1]. From the constants given by Zürich, example values were generated for fibre volume fractions of 0.45, 0.50 and 0.55. For G0986, Douai measured single values at different V_f using the through-thickness compression method, which are plotted in Fig. 1 (K_1 for G0986). The most obvious observation is that there is a very significant scatter of results, with values for K_1 and K_2 at any given fibre volume fraction varying by up to one order of magnitude. Even results obtained using virtually identical procedures show significant scatter, as illustrated by the data for G0986 submitted by Clausthal, Douai (linear sat.), Lausanne and ONERA (Table 7). While all determined the permeability from measurement of the mass flow in linear saturated flow experiments at constant injection pressure and evaluation of the raw data based on Eq. (5), the results differ significantly.

Two well known and well documented sources of scatter in measured permeability data are experimental errors and material variability. Experimental errors are uncertainties in each individual experiment for permeability measurement, induced by the limited accuracy of the experimental set-up. Based on the equations for evaluation of the raw data, the effective experimental error can be determined from the uncertainties of the input data according to the law of error propagation [18,49]. For the example of saturated linear flow as described in Eq. (5), the experimental error of the measured permeability is

$$\frac{\sigma_K}{\overline{K}} = \pm\sqrt{\left(\frac{\sigma_Q}{\overline{Q}}\right)^2 + \left(\frac{\sigma_\eta}{\overline{\eta}}\right)^2 + \left(\frac{\sigma_L}{\overline{L}}\right)^2 + \left(\frac{\sigma_{\Delta p}}{\overline{\Delta p}}\right)^2 + \left(\frac{\sigma_A}{\overline{A}}\right)^2}, \tag{8}$$

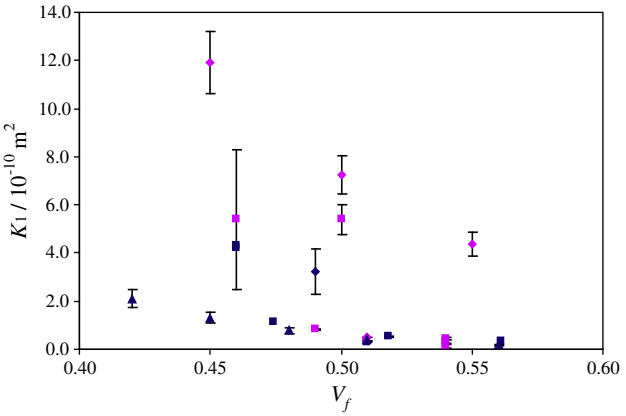

Fig. 1. G0986: Measured principal permeability value K_1 as a function of the fibre volume fraction V_f. Different symbols indicate experimental method (dark diamond: radial unsat.; light diamond: radial sat.; dark square: linear unsat.; light square: linear sat.; dark triangle: 1D compression).

where the expressions in the brackets describe the uncertainties in determination of the respective quantities. Similarly, the experimental error of the permeability determined from unsaturated radial flow experiments according to Eq. (6) is

$$\frac{\sigma_K}{\overline{K}} = \pm\sqrt{\left(\frac{\sigma_\Phi}{\overline{\Phi}}\right)^2 + \left(\frac{\sigma_\eta}{\overline{\eta}}\right)^2 + 4\left(\frac{\sigma_{R_0}}{\overline{R_0}}\right)^2 + \left(\frac{\sigma_{\Delta p}}{\overline{\Delta p}}\right)^2 + \left(\frac{\sigma_{t_{ff}}}{\overline{t_{ff}}}\right)^2 + \left(\frac{\sigma_F}{\overline{F}}\right)^2}, \tag{9}$$

[1] For interpretation of colour in Figs. 1–6, the reader is referred to the web version of this article.

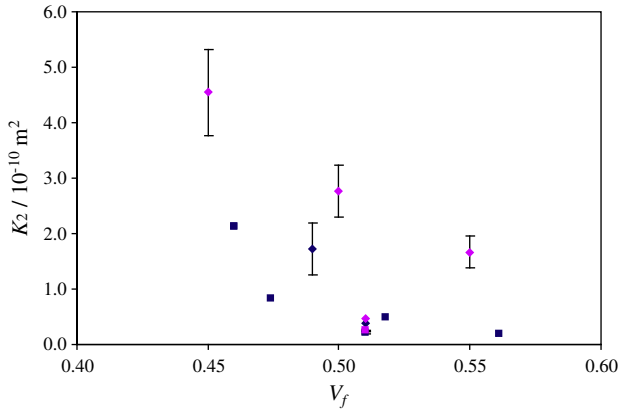

Fig. 2. G0986: Measured principal permeability value K_2 as a function of the fibre volume fraction V_f. Different symbols indicate experimental method (dark diamond: radial unsat.; light diamond: radial sat.; dark square: linear unsat.; light square: linear sat.).

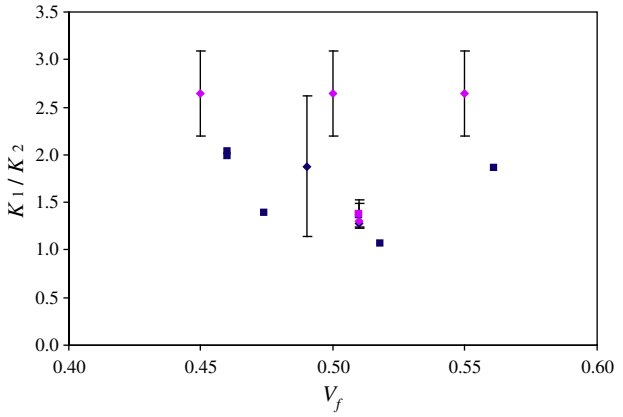

Fig. 3. G0986: Ratio of measured principal permeability values K_1 and K_2 as a function of the fibre volume fraction V_f. Different symbols indicate experimental method (dark diamond: radial unsat.; light diamond: radial sat.; dark square: linear unsat.; light square: linear sat.).

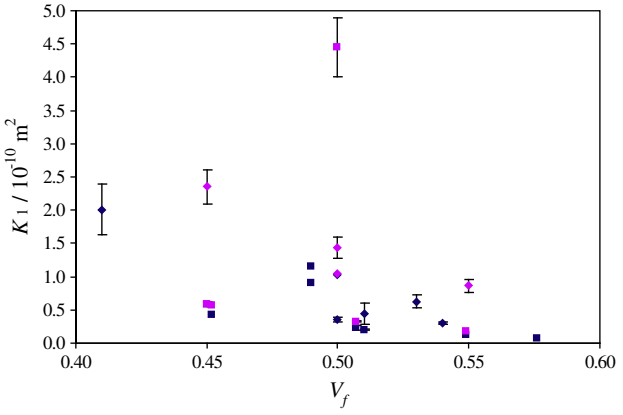

Fig. 4. 01113: Measured principal permeability value K_1 as a function of the fibre volume fraction V_f. Different symbols indicate experimental method (dark diamond: radial unsat.; light diamond: radial sat.; dark square: linear unsat.; light square: linear sat.).

where

$$F = \left(\frac{R_{ff}}{R_0}\right)^2 \left(2\ln\left(\frac{R_{ff}}{R_0}\right) - 1\right) + 1. \quad (10)$$

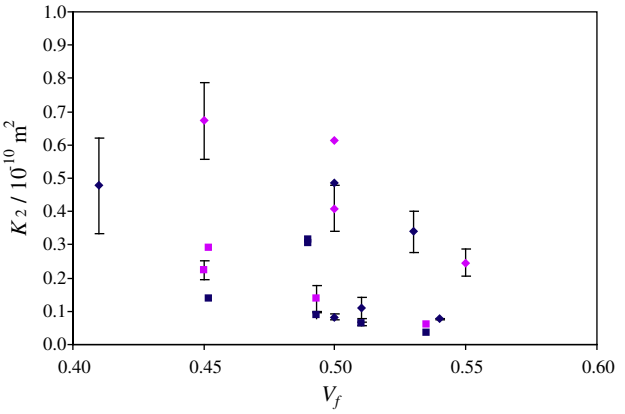

Fig. 5. 01113: Measured principal permeability value K_2 as a function of the fibre volume fraction V_f. Different symbols indicate experimental method (dark diamond: radial unsat.; light diamond: radial sat.; dark square: linear unsat.; light square: linear sat.).

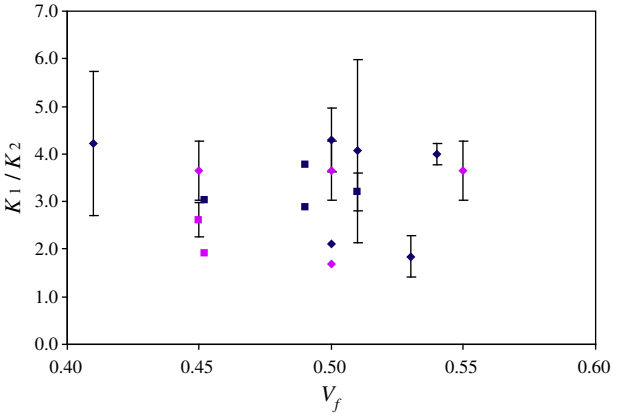

Fig. 6. 01113: Ratio of measured principal permeability values K_1 and K_2 as a function of the fibre volume fraction V_f. Different symbols indicate experimental method (dark diamond: radial unsat.; light diamond: radial sat.; dark square: linear unsat.; light square: linear sat.).

The uncertainty in F can be determined statistically following the method suggested by Heardman et al. [49]. Based on similar considerations, experimental errors can be easily derived for the methods described in Eqs. (2) and (7). For a series of N_{exp} experiments, the contribution of the error in each individual experiment to the observed variability in permeability is reduced by a factor $N_{exp}^{-1/2}$. It was recommended that all participants quantify experimental uncertainties inherent to the procedures they implement.

In addition, scatter of the results is caused by the fact that no two specimens are identical. All textile fabrics show in general some degree of non-uniformity, which affects the local permeability and contributes to the uncertainty in measured global permeability values. Local variations in fibre spacing and fibre angle are inherent to any fabric architecture. They may also be induced by effects of gravity and handling during storage and transport, as well as by cutting, stacking and shearing of fabric layers during preform preparation. Eventually, fabric properties, in particular V_f and fibre orientations, may vary between material batches and specimens. Effects such as layer misalignment and nesting may contribute to the variability in permeability of multilayer specimens. It was found before that the influence of specimen variability on the scatter in measured permeability values tends to be higher than the influence of the experimental error [13]. Because of the variability in specimen properties, all permeability data

should be based on experiments on more than one specimen. Repeated measurement on the same specimen, which is possible in saturated flow experiments, does not reflect the variability and thus may be misleading.

To avoid effects of specimen variability in benchmarking of permeability measurement methods, use of a reference medium for calibration was suggested [50,51]. This could be manufactured with high geometrical accuracy from a rigid material to obtain reproducibility of the pore structure. Single-scale porosity would allow effects of partial saturation to be avoided, thus minimising differences in results of saturated and unsaturated flow experiments. If available, specimens of this type could be used in future work.

However, differences in results of one order of magnitude cannot be explained by experimental errors and the influence of fabric non-uniformity (which, combined, are typically in the range of 20–30%; here, the maximum is 63%), but can only be explained by human factors. Most severe are potential misconceptions about the measurement procedure and implementation of unsuitable equations for data reduction, which may result in invalid results, even if the acquired raw data are valid. An example is assumption of isotropic behaviour, when in fact the fabric properties are anisotropic. Additional sources of scatter can be different definitions for the permeability and their inconsistent use, in particular related to the factor $1/\Phi$ between Darcy velocity and flow front velocity, and inconsistent use of units (e.g. cm–m, metric–imperial). Inconsistent specimen preparation (e.g. lay-up sequence, layer orientation) can also contribute to differences in measured values. The information given in Tables 3–6 indicates which of the implemented procedures may be affected by systematic issues related to the design of the experimental set-up discussed above.

3.2. Specific observations

The large scatter on the absolute values of K_1 and K_2, which determine the mould fill time, is considered a secondary problem. More critical for practical application is the ratio of the principal permeability values, since it determines the mould filling pattern and thus is of high relevance for tool design, in particular location of injection gates and vents. For the example of 01113, quoted average values of K_1/K_2, varying between 1.8 and 4.3, are expected to result in significantly different flow front shapes, which may have severe implications for tool design.

Despite the large scatter, all results tend to agree on the following:

- The main flow direction is oriented along the fabric weft direction for G0986, along the warp direction for 01113.
- Both K_1 and K_2 are higher for G0986 than for 01113.
- The same applies to the ratio K_1/K_2, i.e. 01113 is more anisotropic than G0986.

Based on the nominal data for characterisation of the fabric architecture (Table 1), G0986 would be expected to be isotropic. It can be speculated that deviation from the ideal behaviour (average values of K_1/K_2 vary between 1.1 and 2.6) may be caused by different yarn cross-sections along both fabric directions (induced by the weaving process), resulting in larger inter-yarn gap spaces in the weft than in the warp direction. For 01113, orientation of the main flow direction along the warp direction is plausible, since the data in Table 1 suggest coarser structure in the warp than in the weft direction. The degree of anisotropy would be expected to be stronger for 01113 than for G0986, which is confirmed by the results.

Comparing average permeability values obtained by different participants, no trends regarding the influence of linear/radial injection, saturated/unsaturated flow or injection at constant pressure/constant flow rate can be identified. Similarly, comparison of the coefficients of variation (where available) does not indicate any trend. This suggests that other factors have a more significant influence on the scatter of measured permeability values and their variability than the experimental method used. While comparison between values from different participants at different fibre volume fractions is hardly possible, participants, who measured the permeability at different V_f, observed an expected decrease in permeability with increasing V_f. This indicates that at least for each procedure individually, results show some consistency, implying that there is some significance to the observed scatter between values obtained by different participants.

Values for the angle θ were quoted explicitly by Montréal, Nottingham and Zürich. The results from Nottingham and Zürich indicate almost perfect alignment of the principal permeability axes with the fabric weft and warp directions, while the results from Montréal show deviations of up to 22° (G0986) and of 15° (01113, Scheme 2). This seems to imply that for determination of the angle θ, radial flow experiments are more robust than linear flow experiments along three fabric directions. In general, this may be related to the issues affecting linear flow experiments (Section 2.1). However, since measures were taken to avoid these issues (the specimen aspect ratio was greater than the ratio of anisotropy of the specimen permeability; specimen edges were sealed to avoid racetracking [46]), it is not quite clear how they may have affected the results here.

Some participants studied specific aspects of permeability measurement. Clausthal, DLR, le Havre and Montréal carried out saturated and unsaturated flow experiments and compared the results. As discussed by Pillai [38], saturated and unsaturated permeabilities of fabrics have been compared in several published studies. The difference between both permeabilities is caused by effects of partial saturation and depends on the ratio between the capillary pressure in the fibre bundles (which depends on the fabric properties) and the applied injection pressure [40]. Since a variety of reinforcements have been tested applying different injection conditions and test fluids, a wide range of observations is documented in the literature on the ratio of saturated and unsaturated permeability, which do not even agree on whether the ratio should be equal to, or greater or smaller than one. Here, the data presented by Clausthal for G0986 suggest that saturated flow experiments result in higher permeability values than unsaturated experiments, and that the difference is greater than the variability (standard deviation) of the results. For 01113, le Havre made similar observations. DLR observed only small differences for both fabrics, from which no clear trend can be identified. Montréal also found that values from saturated experiments are higher than those from unsaturated experiments for G0986, but that the difference is smaller than the variability. In summary, there is a trend for the saturated permeability to be higher than the unsaturated permeability.

Douai compared two methods, linear saturated flow and radial saturated flow in through-thickness compression, for G0986. The quoted average permeability value measured in linear saturated flow along the weft direction at $V_f = 0.49$ is approximately 5% higher than the value measured in radial through-thickness compression at $V_f = 0.48$. This suggests satisfactory agreement between the results from both methods, in particular when the standard deviations for both data points are considered. The agreement is significantly better here than in a recent paper [42], where values from the radial through-thickness compression method were found to be twice as high as those from saturated linear injection experiments at constant injection pressure, although they were in very good agreement with results from radial injection experiments at constant flow rate.

Montréal implemented two different correction schemes to normalise measured permeability values (at slightly varying fibre volume fractions) to the target fibre volume fraction. Both give slightly different results, in particular for 01113. The maximum difference for K_1 or K_2 is 21%, and for the ratio K_1/K_2 it is 24%. Similarly, both schemes give different values of θ (for 01113).

At identical fibre volume fraction, ONERA investigated the influence of the number of layers in the specimen on the measured permeability value for G0986. Based on Eq. (4), this was achieved by varying the number of layers and cavity height to keep V_f constant for the injection experiments. The quoted results suggest a decrease (of the average values) by 36% from one layer to two layers. From two layers to eight layers, the average values decrease by 47%, although this cannot be considered significant due to the high variability of the data. A decrease in permeability with increasing number of fabric layers may be related to different pore geometries between fabric and cavity surface and between adjacent fabric layers in multilayer specimens. Locally increased pore space may result in enhanced flow on the specimen surfaces and thus in increased measured specimen permeability. The influence of effects at the fabric-mould interface on the specimen properties can be expected to decrease with increasing specimen thickness. The permeability of multilayer specimens may also be affected by nesting, which refers to (partial) filling of inter-yarn voids on the surface of a layer by yarns of an adjacent layer. Depending on the fabric architecture, in particular the yarn packing density in each layer [52], and layer alignment, this effect can be significant. At identical V_f, different nesting configurations are possible, which affect the fabric compaction level and thus the permeability, resulting in increased variability [53]. For random nesting, this is expected to have a maximum at two layers [52] and to decrease with increasing number of layers. Here, the coefficient of variation of the measured permeability values increases with increasing number of layers, but it is to be considered that the number of experiments at eight layers is lower than at one and two layers, which may affect the observed variability.

Zürich carried out flow experiments at three different injection pressure values. They suspect that increase of the volume flow (i.e. increased injection pressure) may result in increased measured permeability values. It has been speculated in the literature that effects like this may occur when Darcy's law is violated due to increasing Reynolds number at high flow velocities [54]. However, the original measured data do not indicate a clear trend for a dependence of the permeability on the injection pressure. For G0986, Montréal found a trend for the permeability along the warp direction to increase by 5% with an increase in injection pressure by one bar. However, the correlation between the original data and the linear trend is weak (coefficient of correlation $R^2 = 0.0133$), and the effect on the measured permeability is not very significant, considering that the coefficient of variation in permeability at the given V_f is 16%.

4. Conclusions

The aim of the international permeability benchmark exercise reported here was to get an overview of the methods for permeability measurement in practical use and the range of results obtained implementing these methods. For two materials, a 2×2 twill weave carbon fibre fabric and a 2×2 twill weave E-glass fibre fabric, 11 participants submitted in-plane permeability data (for either one or both materials), which were obtained using a total of 16 different procedures. In summary, most procedures were based on linear injection geometries, most used constant injection pressure, and most measured the permeability in saturated flow experiments. Oils of different specifications were the most frequently used test fluids.

The permeability data suggest that for each procedure, the results are consistent. Regarding comparison of both fabrics, all participants who obtained data for both found similar trends. However, the main finding of the study is that, for each fabric, the results quoted by different participants for the principal permeability values at any given fibre volume fraction show very significant scatter of up to one order of magnitude. The ratio of the principal permeability values, which determines the mould filling pattern and thus is of high relevance for design of tools for LCM processes, varies by factors of up to 2. While the scatter in results from any single series of experiments is affected by experimental uncertainties and variability of the specimens, it is suspected that the main source of the scatter in results from different participants is related to human factors. This implies that the ability to provide consistent permeability data depends on the availability of skilled and experienced personnel for experimental design, reproducible preparation of specimens, operation of equipment and evaluation of measured raw data.

While it is hardly possible to tell which results characterise the material properties most accurately, they cannot all be equally valid. The implemented procedures need to be checked for systematic errors. In addition, procedures need to be put in place to monitor and control tool deflection, test fluid viscosity and injection pressure/flow rate, which can be identified as particularly critical for accurate permeability measurement. To allow interpretation of the results, the measurement procedures need to be fully documented, including quantification of experimental uncertainties.

Aiming at standardisation of measurement procedures and interchangeability of results, prescription of a testing method and a design for testing equipment is currently not considered. However, at least some means of quality management needs to be put in place. Based on the outcomes of this exercise, "good practice" guidelines will be formulated in order to eliminate sources of scatter. These will be implemented in a second benchmark exercise, in which experimental conditions (e.g. fibre volume fraction, number of layers in specimen, number of repeats/number of specimens) will be prescribed, thus allowing more quantitative comparison between results.

References

[1] Darcy H. Les Fontaines Publiques de la Ville de Dijon. Paris: Victor Dalmont; 1856.
[2] Carman PC. Fluid flow through granular beds. Trans Inst Chem Eng – Lond 1937;15:150–6.
[3] Gebart BR. Permeability of unidirectional reinforcements for RTM. J Compos Mater 1992;26(8):1100–33.
[4] Cai Z, Berdichevsky AL. An improved self-consistent method for estimating the permeability of a fiber assembly. Polym Compos 1993;14(4):314–23.
[5] Van der Westhuizen J, Du Plessis JP. An attempt to quantify fibre bed permeability utilizing the phase average Navier–Stokes equation. Compos Part A – Appl Sci 1996;27(4):263–9.
[6] Woerdeman DL, Phelan FR, Parnas RS. Interpretation of 3-D permeability measurements for RTM modeling. Polym Compos 1995;16(6):470–80.
[7] Nordlund M, Lundström TS, Frishfelds V, Jakovics A. Permeability network model for non-crimp fabrics. Compos Part A – Appl Sci 2006;37(6):826–35.
[8] Simacek P, Neacsu V, Advani SG. A phenomenological model for fiber tow saturation of dual scale fabrics in liquid composite molding. Polym Compos 2010;31(11):1881–9.
[9] Endruweit A, Long AC. A model for the in-plane permeability of triaxially braided reinforcements. Compos Part A – Appl Sci 2011;42(2):165–72.
[10] Verleye B, Klitz M, Croce R, Roose D, Lomov S, Verpoest I. Computation of permeability of textile reinforcements. In: Zeng X, Li Y, Ruan D, Koehl L, editors. Studies in computational intelligence. Computational textile. Berlin: Springer; 2007. p. 93–109.
[11] Sharma S, Siginer DA. Permeability measurement methods in porous media of fiber reinforced composites. Appl Mech Rev 2010;63(2) [article no. 020802].
[12] Parnas RS, Howard JG, Luce TL, Advani SG. Permeability characterization. Part 1: A proposed standard reference fabric for permeability. Polym Compos 1995;16(6):429–45.
[13] Lundström TS, Stenberg R, Bergström R, Partanen H, Birkeland PA. In-plane permeability measurements: a Nordic round-robin study. Compos Part A – Appl Sci 2000;31(1):29–43.

[14] Luo Y, Verpoest I, Hoes K, Vanheule M, Sol H, Cardon A. Permeability measurement of textile reinforcements with several test fluids. Compos Part A – Appl Sci 2001;32(10):1497–504.
[15] Lundström TS, Gebart BR, Sandlund E. In-plane permeability measurements on fiber reinforcements by the multi-cavity parallel flow technique. Polym Compos 1999;20(1):146–54.
[16] Ahn SH, Lee WI, Springer GS. Measurement of the three-dimensional permeability of fiber preforms using embedded fiber optic sensors. J Compos Mater 1995;29(6):714–33.
[17] Weitzenböck JR, Shenoi RA, Wilson PA. Measurement of three-dimensional permeability. Compos Part A – Appl Sci 1998;29(1–2):159–69.
[18] Endruweit A, McGregor P, Long AC, Johnson MS. Influence of the fabric architecture on the variations in experimentally determined in-plane permeability values. Compos Sci Technol 2006;66(11–12):1778–92.
[19] Luthy T, Landert M, Ermanni P. 1D-permeability measurements based on ultrasound and linear direct current resistance monitoring techniques. J Mater Process Manuf 2001;10(1):25–43.
[20] Ferland P, Guittard D, Trochu F. Concurrent methods for permeability measurement in resin transfer molding. Polym Compos 1996;17(1):149–58.
[21] Verheus AS, Peeters JHA. The role of reinforcement permeability in resin transfer moulding. Compos Manuf 1993;4(1):33–8.
[22] Adams KL, Rebenfeld L. In-plane flow of fluids in fabrics: structure/flow characterization. Text Res J 1987;57(11):647–54.
[23] Adams KL, Russel WB, Rebenfeld L. Radial penetration of a viscous liquid into a planar anisotropic porous medium. Int J Multiphase Flow 1988;14(2):203–15.
[24] Chan AW, Hwang ST. Anisotropic in-plane permeability of fabric media. Polym Eng Sci 1991;31(16):1233–9.
[25] Weitzenböck JR, Shenoi RA, Wilson PA. Radial flow permeability measurement. Part A: Theory. Compos Part A – Appl Sci 1999;30(6):781–96.
[26] Weitzenböck JR, Shenoi RA, Wilson PA. Radial flow permeability measurement. Part B: Application. Compos Part A – Appl Sci 1999;30(6):797–813.
[27] Chan AW, Larive DE, Morgan RJ. Anisotropic permeability of fiber preforms: constant flow rate measurement. J Compos Mater 1993;27(10):996–1008.
[28] Young WB, Wu SF. Permeability measurement of bidirectional woven glass fibers. J Reinf Plast Comp 1995;14(10):1108–20.
[29] Han KK, Lee CW, Rice BP. Measurements of the permeability of fiber preforms and applications. Compos Sci Technol 2000;60(12–13):2435–41.
[30] Parnas RS, Salem AJ. A comparison of the unidirectional and radial in-plane flow of fluids through woven composite reinforcements. Polym Compos 1993;14(5):383–94.
[31] Gebart BR, Lidström P. Measurement of in-plane permeability of anisotropic fiber reinforcements. Polym Compos 1996;17(1):43–51.
[32] Weitzenböck JR, Shenoi RA, Wilson PA. Measurement of principal permeability with the channel flow experiment. Polym Compos 1999;20(2):321–35.
[33] Tan H, Pillai KM. Effect of fiber-mat anisotropy on 1D mold filling in LCM: a numerical investigation. Polym Compos 2008;29(8):869–82.
[34] Bickerton S, Advani SG, Mohan RV, Shires DR. Experimental analysis and numerical modeling of flow channel effects in resin transfer molding. Polym Compos 2000;21(1):134–53.
[35] Lundström TS, Toll S, Hakanson JM. Measurement of the permeability tensor of compressed fibre beds. Trans Porous Med 2002;47(3):363–80.
[36] Lawrence JM, Barr J, Karmakar R, Advani SG. Characterization of preform permeability in the presence of race tracking. Compos Part A – Appl Sci 2004;35(12):1393–405.
[37] Wang TJ, Wu CH, Lee LJ. In-plane permeability measurement and analysis in liquid composite molding. Polym Compos 1994;15(4):278–88.
[38] Pillai KM. Modeling the unsaturated flow in liquid composite molding processes: a review and some thoughts. J Compos Mater 2004;38(23): 2097–118.
[39] Palmese GR, Karbhari VM. Effects of sizings on microscopic flow in resin transfer molding. Polym Compos 1995;16(4):313–8.
[40] Ahn KJ, Seferis JC, Berg JC. Simultaneous measurements of permeability and capillary pressure of thermosetting matrices in woven fabric reinforcements. Polym Compos 1991;12(3):146–52.
[41] Hoes K, Dinescu D, Sol H, Vanheule M, Parnas RS, Luo Y, et al. New set-up for measurement of permeability properties of fibrous reinforcements for RTM. Compos Part A – Appl Sci 2002;33(7):959–69.
[42] Comas-Cardona S, Binetruy C, Krawczak P. Unidirectional compression of fibre reinforcements. Part 2: A continuous permeability tensor measurement. Compos Sci Technol 2007;67(3–4):638–45.
[43] Verrey J. Resin transfer moulding of complex shaped composites using carbon fibre non-crimp fabrics. PhD thesis no. 3003, EPF Lausanne; 2004.
[44] Gommer F. Permeability of textile reinforcements: benchmark measurements. Master thesis. KU Leuven; 2007.
[45] Gommer F, Vanderbosch K, Lomov SV, Verpoest I. Error assessment in permeability measurement using radial flow method. Adv Compos Lett 2009;18(4):121–3.
[46] Demaria C, Ruiz E, Trochu F. In-plane anisotropic permeability characterization of deformed woven fabrics by unidirectional injection. Part I: Experimental results. Polym Composite 2007;28(6):797–811.
[47] Laine B, Boust F, Boisse P, Hivet G, Lomov S, Fanget A. Perméabilité des renforts fibreux: étude des écarts expériences-prédictions. Revue des Composites et des Matériaux Avancés 2005;15(3):385–400.
[48] Arbter R. Contribution to robust resin transfer molding. Dissertation no. 18108, ETH Zürich; 2008.
[49] Heardman E, Lekakou C, Bader MG. Flow monitoring and permeability measurement under constant and transient flow conditions. Compos Sci Technol 2004;64(9):1239–49.
[50] Morren G, Gu J, Sol H, Verleye B, Lomov S. Stereolithography specimen to calibrate permeability measurements for RTM flow simulations. Adv Compos Lett 2006;15(4):119–25.
[51] Vechart AP, Masoodi R, Pillai KM. Design and evaluation of an idealized porous medium for calibration of permeability measuring devices. Adv Compos Lett 2010;19(1):35–49.
[52] Lomov SV, Verpoest I, Peeters T, Roose D, Zako M. Nesting in textile laminates: geometrical modelling of the laminate. Compos Sci Technol 2003;63(7): 993–1007.
[53] Hoes K, Dinescu D, Sol H, Parnas RS, Lomov S. Study of nesting induced scatter of permeability values in layered reinforcement fabrics. Compos Part A – Appl Sci 2004;35(12):1407–18.
[54] Kim SK, Daniel IM. Observation of permeability dependence on flow rate and implications for liquid composite molding. J Compos Mater 2007;41(7):837–49.